6878 *Macromolecules* **2009**, *42*, 6878–6884
DOI: 10.1021/ma901142g

Macromolecules
ARTICLE

Graphitic Nanoribbons with Dibenzo[*e*,*l*]pyrene Repeat Units: Synthesis and Self-Assembly

Yulia Fogel,[†] Linjie Zhi,[†,‡] Ali Rouhanipour,[†] Denis Andrienko,[†] Hans Joachim Räder,[†] and Klaus Müllen*,[†]

[†]*Max Planck Institute for Polymer Research, Ackermannweg 10, D-55128 Mainz, Germany, and* [‡]*National Center for Nanoscience and Technology, Zhongguancun, Beiyitiao, 11, 100080 Beijing, P. R. China*

Received May 26, 2009; Revised Manuscript Received August 12, 2009

ABSTRACT: A novel homologous series of five monodisperse ribbon-type polyphenylenes, with rigid dibenzo[*e*,*l*]-pyrene cores in the repeat units, are synthesized by a microwave-assisted Diels−Alder reaction. The size of the obtained polyphenylene ribbons ranges from 132 to 372 carbon atoms in the aromatic backbone which incorporates up to six dibenzo[*e*,*l*]pyrene units, thus showing quite different aspect ratios. Because of the flexibility of the backbone and the peripheral substitution with dodecyl chains, the polyphenylene ribbons are well soluble in organic solvents and can be fully characterized by standard analytical techniques. Their unique structure is especially designed to produce a series of giant ribbon-type polycyclic aromatic hydrocarbons (PAHs) in a single further reaction step by cyclodehydrogenation. Therefore, the incorporated dibenzo[*e*,*l*]pyrene cores are an important feature because they facilitate the dehydrogenation and improve the reaction yields. The smallest representative of the completely dehydrogenated planarized (2D) PAH ribbons, prepared from the polyphenylene ribbon with 132 aromatic carbon atoms, is still sufficiently soluble and shows a λ_{max} value of 644 nm. Most importantly, these graphitic molecules self-organize into 2D columns when adsorbed on highly oriented pyrolytic graphite (HOPG), thus rendering them attractive candidates for future applications in organic electronic devices such as e.g. field effect transistors. A deeper insight into possible conformations of the sterically demanding side chains and their influence on the packing behavior of such giant PAHs into columnar arrangements is additionally obtained by molecular dynamics simulations. Using Marcus theory for a nonadiabatic temperature-activated charge transfer, we discuss the advantages of an extended, anisotropic in shape, π-system as compared to traditional one-dimensional molecular arrangements of typical discotics.

Introduction

Polycyclic aromatic hydrocarbons (PAHs) are well-defined "pieces of graphite" which own a size-dependent adjustable redox behavior. A representative example of PAHs is hexa-*peri*-hexabenzocoronene (HBC)[1−3] which can be exploited in organic electronic devices such as field-effect transistors, injection layers, or solar cells.[4,5] The success of such devices is determined by two important factors: (i) the electronic properties of the individual organic molecules and (ii) their ability to form stable supramolecular structures with an appropriate alignment for the desired application. Therefore, the spontaneous formation of uniform large-area structures by individual PAH self-assembly is of key importance for material science and organic electronics.[6−8] Additionally, a unique feature of self-assembled structures is the ability of self-healing to produce defect-free arrangements on a supramolecular level which is also imperative for organic electronics. It is their general tendency to aggregate via $\pi-\pi$ orbital interactions that uniquely dictates the form or pattern of the final supramolecular structure.[9,10]

PAH-based *double-stranded* or *ribbon-type* polymers had sparked the attention of several research groups (Air Force Materials Laboratory,[11−14] Stille,[15−17] and Marvel[18,19]) in the early 1960s. These materials fill the gap between single-stranded (one-dimensional) conjugated polymers and two-dimensional graphitic sheets and combine useful characteristics of both. The ribbon-type structures have a two-dimensional, essentially planar conformation, resulting in a high delocalization of electrons along the backbone and, correspondingly, high charge carrier mobilities, similar to ladder-type conjugated polymers.[20,21] However, in spite of their unique material properties, the synthesis and characterization of defect-free, soluble hydrocarbon ribbon polymers is still one of the ongoing challenges in synthetic chemistry.

A great number of two-dimensional soluble giant PAHs with different shapes and sizes have been prepared in our group,[5,21−29] and several individual procedures for their synthesis have been discovered.[30−33] Our general strategy of PAH production has two important steps: first, the design and synthesis of soluble polyphenylene precursor molecules and, second, the formation of aromatic C−C bonds by cyclodehydrogenation. Thus, appropriate polyphenylene precursor structures can be converted in a single reaction step into the desired planarized PAH structures. On the basis of this concept, we present a unique solution to synthesize a new homologous series of monodisperse soluble polyphenylenes, the so-called polyphenylene ribbons which serve as precursors for completely dehydrogenated "graphitic" PAH nanomolecules, so-called PAH ribbons. Therefore, we developed a series of five well-defined monodisperse polyphenylene ribbons with increasing length containing up to six dibenzo[*e*,*l*]pyrene units in a three-dimensional backbone (see Scheme 3). In spite of the apparent backbone flexibility due to the linkage of the dibenzo[*e*,*l*]pyrene units by "zigzag" bonded biphenyl bridges, the polyphenylene ribbons are expected to have a quasi-rigid linear structure because of the steric hindrance between the neighboring stiff and bulky dibenzo[*e*,*l*]pyrene units. As these new molecules are monodisperse, they offer the advantage of owning reproducible physicochemical properties, and their rigid moieties with a predefined topology seem to be the key feature for a successful cyclodehydrogenation toward large PAH ribbons.

*Corresponding author: e-mail muellen@mpip-mainz.mpg.de.

 Published on Web 08/28/2009

Results and Discussion

To introduce rigid pyrene moieties into a polyphenylene ribbon core, 2,7-di-*tert*-butyl-4,5:9,10-bis(2,5-di-*p*-dodecylphenylcyclopenta)[*e*,*l*]pyren-5,11-dione (**2**) was used as a building block (Scheme 1). Applying the Knoevenagel condensation between **1** and 1,3-bis(4-*n*-dodecylphenyl)propan-2-one was furnished in 60% yield. Modification of the previously reported reaction conditions for the preparation of **2** led to a significant increase in the reaction yield.[32]

Scheme 1. Synthesis of the Key Building Blocks 2,7-Di-*tert*-butyl-4,5:9,10-bis(2,5-di-*p*-dodecylphenylcyclopenta)[*e*,*l*]pyren-5,11-dione (2) and 1,2,3,4-Tetra-(4-dodecylphenyl)-5-(2′-ethynylbiphen-2-yl) (5)[a]

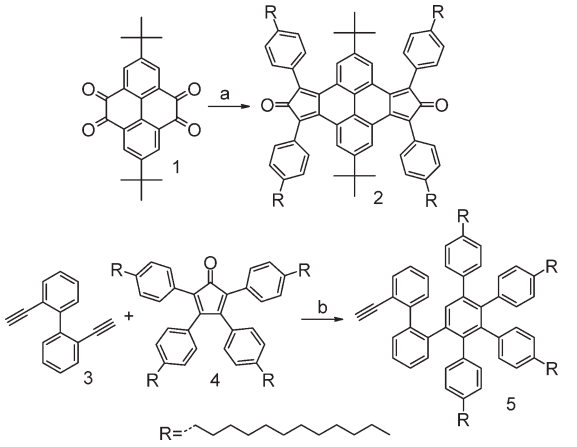

[a] Reagents and conditions: (a) KOH, EtOH, 1,3-bis(4-*n*-dodecylphenyl)propan-2-one, 3 h, 50 °C, 60%; (b) toluene, 110 °C, 46%.

The second building block, 1,2,3,4-tetra-(4-dodecylphenyl)-5-(2′-ethynylbiphen-2-yl) (**5**), was synthesized via Diels−Alder reaction between **3** and **4** (Scheme 1). The use of toluene as a solvent together with a lower reaction temperature was found to be beneficial in terms of the yield. The Diels−Alder reaction between the precursors **2** and **5** (Scheme 2) was carried out in a microwave apparatus (300 W and cooling in toluene at 110 °C for 1 h) with varying stoichiometries. The novelty of such a Diels−Alder reaction is that two required structures can be synthesized in a single step, simply by adjusting an appropriate stoichiometry for the precursors **2** and **5** in order to obtain the desired ratio between the two reaction products **6** and **7**, where **7** is the first and smallest polyphenylene ribbon containing 132 skeletal atoms in the aromatic core and **6** is the starting compound for the next higher homologue polyphenylene ribbon **9**. The two products are separated by column chromatography using a gradient mixture of petroleum ether and dichloromethane as an eluent. Next, the second generation of molecules, polyphenylene ribbon **9** and compound **8**, are obtained by stoichiometrically controlled cycloaddition of **6** and **3** with subsequent chromatographic separation. Thereby, molecule **8** serves as the starting compound for the third generation of polyphenylene ribbon **11**. Analogously, by applying this novel Diels−Alder protocol, a homologues series of five polyphenylene ribbons (**7**, **9**, **11**, **13**, and **15**) with different aspect ratios were synthesized, and the largest, **15**, contains 372 carbon atoms in the aromatic

Scheme 2. Diels−Alder Synthetic Protocol toward the Successive Synthesis of a Homologous Series of Five Polyphenylene Ribbons[a]

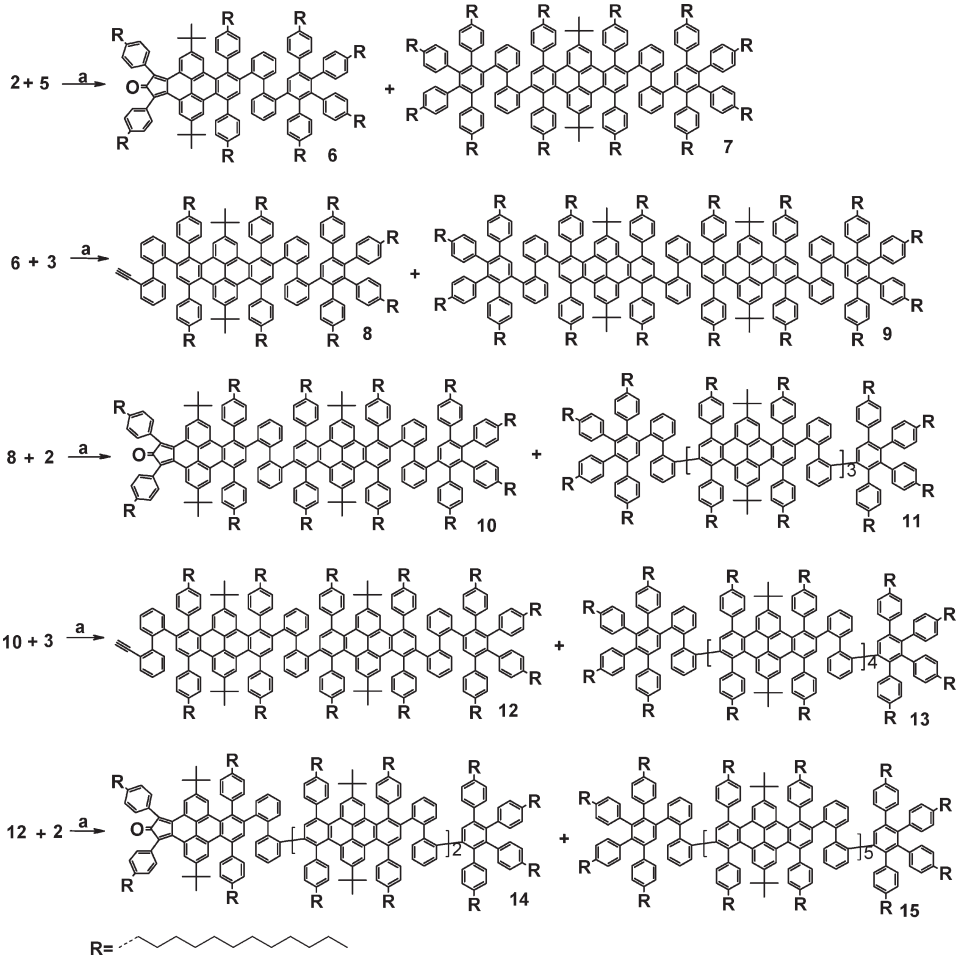

[a] Reagents and conditions: (a) CEM Discover microwave at 300 W with cooling, toluene, 110 °C, 1 h.

core and has a molecular weight of 9974 g/mol (Scheme 3), thus being the precursor of a giant PAH which implies a central acene structure with 36 linearly fused benzene rings. Synthetic details as well as spectroscopic structure analysis for all compounds are included in the Supporting Information.

All the synthesized polyphenylene ribbons **7**, **9**, **11**, **13**, and **15** possess very good solubility in common organic solvents, and their characterization was performed by using standard analytical techniques. Characterization by MALDI-TOF mass spectrometry (using dithranol as a matrix) and NMR spectroscopy unequivocally proved the proposed molecular structures (see Supporting Information). Analysis by gel permeation chromatography showed the monodisperse nature of the polyphenylene ribbons, and high-performance liquid chromatography confirmed the purity of the products.

These polyphenylene ribbons can be converted to the desired PAH ribbons in a single further reaction step by cyclodehydrogenation. Whereas this type of reaction works analogously for the whole homologous series of precursor molecules, the higher homologues, however, bear the drawback that their characterization is very much hampered. The purity check by MALDI-TOF mass spectrometry, for example, can be successfully used for the smallest homologue **16** but fails for the higher molecular weight PAH ribbons because of ample fragmentation during measurement. Thus, in the following we focus on the synthesis and characterization of PAH **16** as representative also for the higher molecular weight PAH ribbons.

Polyphenylene ribbon **7** was submitted to cyclodehydrogenation using anhydrous $FeCl_3$ as both an oxidant and a Lewis acid in order to obtain the PAH ribbon **16** (Scheme 4). As was reported previously, the cyclodehydrogenation of **17** (Scheme 4) showed a reduced purity, expressed by the presence of different partially fused species.[32] This drawback led to the design of compound **18**, where the presence of a dibenzo[*e,l*]pyrene unit in the precursor molecule (Scheme 4, blue segments) facilitates a complete cyclodehydrogenation toward the corresponding PAH

Scheme 3. Homologous Series of Polyphenylene Ribbons: C132 (7)−C372 (15)

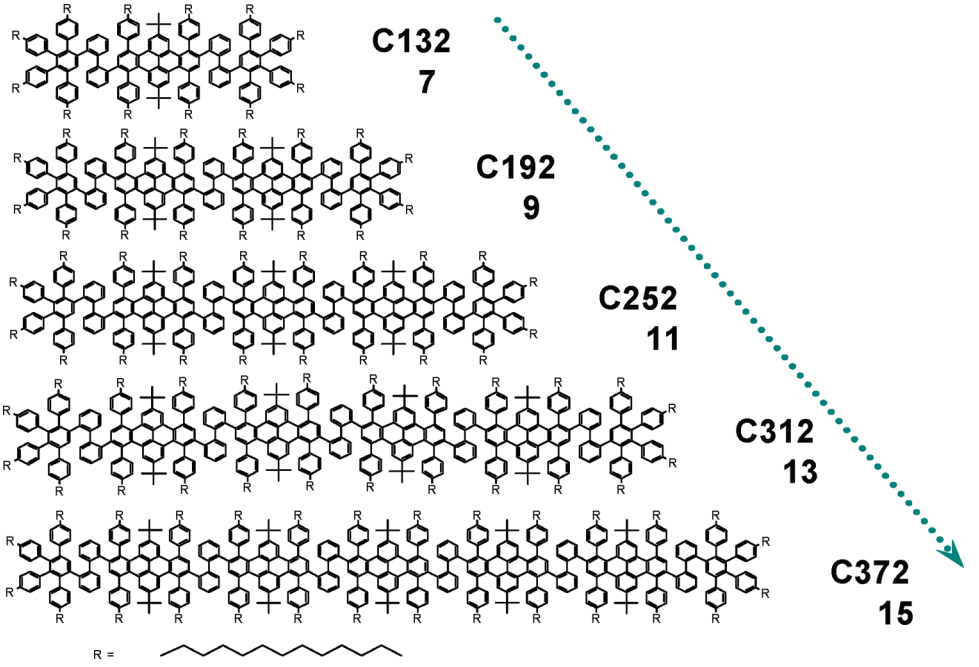

Scheme 4. Cyclodehydrogenation of Polyphenylene Ribbon 7 toward the "Graphitic" PAH Ribbon 16[a]

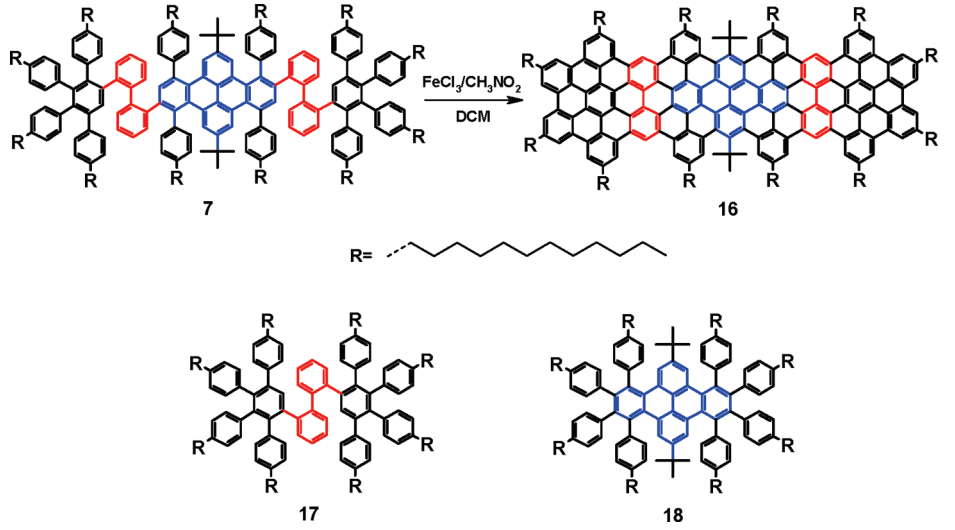

[a] Reaction conditions: $FeCl_3/CH_3NO_2$, DCM, room temperature, 20 h, under steam of argon; schematic presentation of compounds **17** and **18**.

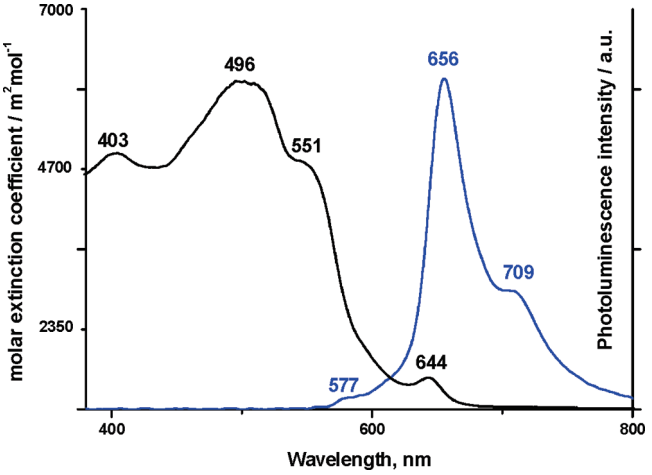

Figure 1. Optical spectra of PAH ribbon **16**, emission excited at 570 nm (2.12×10^{-5} mol/L) in THF at room temperature.

molecule.[32] Structural extension of **17** into **18**, which results in the design of compound **7**, was the main improvement for the fusing process and yielded the PAH ribbon **16** after complete cyclodehydrogenation.

The PAH ribbon **16** was obtained as a dark red solid in 80% yield, being reasonably well soluble in organic solvents such as THF and toluene at room temperature. Therefore, its purification was conducted chromatographically. The good solubility is caused by the presence of many solubilizing long alkyl chains and the slight distortion of the aromatic core from planarity by bulky *tert*-butyl groups. This concept was developed recently in our group and was used for the solubilization of extended or heteroatom-containing PAHs.[30−32]

The MALDI-TOF mass spectrum showed the molecular ion of **16** at 3759 Da which fits very well to the calculated molecular weight of 3759.92 g/mol for this structure with the composition $C_{284}H_{346}$. Additionally, the molecular ion could be measured with isotopic resolution and exhibits good agreement with the simulated isotopic pattern.

The UV/vis spectrum of **16** (Figure 1), recorded in THF at room temperature with a concentration of 2.12×10^{-5} mol/L, shows a number of transition bands (α, β, and p)[34,35] typical for PAHs and a more than 3 times higher molar extinction coefficient relative to HBC. To label the bands and determine their excitation energies, **16** was first optimized using the Becke three-parameter Lee−Yang−Parr (B3LYP) functional and 6-31G(d,p) basis set. Zerner's intermediate neglect of differential overlap (ZINDO) method was then used to calculate the first 10 excited states. All theoretical work was performed using the GAUSSIAN package.[36] The results show good agreement with the experimentally determined peak positions (Table 1), and the error is within the expected range for this method.[37] According to the simulation, the band at 644 nm corresponds to the α-transition. The β-band (the most intense) has the lowest wavelength of 496 nm. The p-band has an intermediate wavelength (551 nm) and intensity which arises from the transition of the highest occupied molecular orbital (HOMO) to the lowest unoccupied molecular orbital (LUMO). The emission spectrum of **16** (Figure 1, blue line) looks less complicated, which can be attributed to the lower symmetry of the PAH ribbon as compared to HBC.

As already mentioned in the Introduction, the ability for self-organization of organic semiconductors on surfaces is an important premise for organic electronic devices; thus, in the following we explore the behavior of PAH ribbon **16** in thin layers by transmission electron microscopy (TEM), selected area electron diffraction (SAED), and scanning tunneling microscopy (STM).

Table 1. Comparison between the Calculated Excitation Energies (E) and Oscillator Strengths (f) and the Experimentally Determined Energies of PAH Ribbon 16

transition	E_{exp} (eV)	E_{calc} (eV)	f_{calc}
a	1.92	2.19[a]	0.0118
p	2.25	2.34[b]	0.0001
b	2.50	2.67	6.38

[a] Wave function composition: 0.38 (H−1 − L+1). [b] Wave function composition: 0.46 (H−1 − L+1).

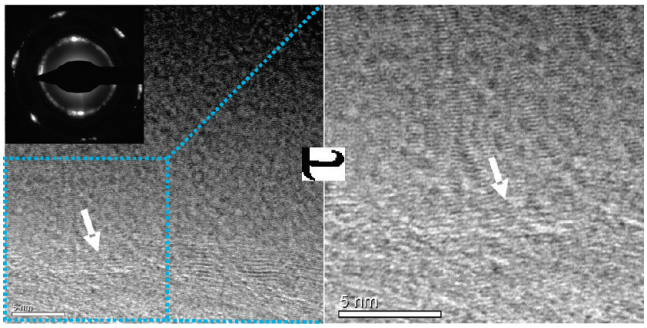

Figure 2. HRTEM images of a film of PAH ribbon **16** obtained by drop-casting of a THF solution. The inset shows the SAED pattern of the film.

Drop-casting of a dilute THF solution of **16** on amorphous carbon-covered copper grids resulted in a thin film of PAH ribbons on the grid surface. Layer-by-layer stacking of the molecules was partially visible under the electron beam of a TEM as shown by the arrows in Figure 2. SAED characterization, however, could not clearly detect the $\pi-\pi$ interaction of the PAH ribbons. The ringlike spots of the diffraction pattern (see the inset of Figure 2a) suggested the existence of two crystal planes corresponding to a *d*-spacing of 0.218 nm {indices (110)} and 0.128 nm {indices (210)}, similar to what has been reported for single- or double-layer graphenes.[38,39] The symmetrical bright areas of the diffraction pattern implied the existence of only a few PAH ribbon layers along the direction of the electron beam, which probably led to the disappearance of the diffraction signal of index (002). The crystal lattice of the (110) plane was clearly observed when the selected area (square marked in Figure 2a) was zoomed in (Figure 2b), in which stacks of ca. 5 PAH ribbon layers were visible as indicated by an arrow.

Figure 3 shows STM images of self-assembled monolayers of PAH ribbon **16** produced by drop-casting of a THF solution on HOPG. After drying, the images were recorded at the solid/liquid interface in dodecane and reveal polycrystalline structures consisting of bright parallel stripes with different orientation in adjacent domains (Figure 3, background picture). These bright stripes correspond to regions with high tunneling current and can be assigned to π-conjugated cores of **16** forming extended columnar structures. On a scale of several tens of nanometers, these stripes adopt a very regular pattern with a spacing of 5 nm (Figure 3, middle-ground picture), and on the nanometer scale an additional structure is visible within the stripes with a periodicity of about 0.4 nm (Figure 3, foreground picture). The latter value can be assigned to the intermolecular distance of the PAH ribbon molecules in a columnar arrangement in which the molecular planes are oriented perpendicular to the HOPG surface and parallel to each other (see the inset in Figure 3). The regular spacing of 5 nm between the columns resembles well the length of about 4.1 nm for the rigid π-system of **16** as obtained from molecular modeling. The aliphatic side chains, which are partially

positioned in the darker parts of the image, could not be resolved, probably because of their high conformational mobility on a time scale faster than the STM imaging.

Columnar structures as determined by STM are promising for electronic applications of PAH ribbon **16**. However, it is not self-evident that such large molecules with extended π-systems as well as their possible higher homologues are still able to self-organize in columns, and it is questionable how the alkyl chains, decorating the aromatic core (invisible in the STM experiment), influence the molecular packing. One can further ask if the principal idea to improve the electronic performance of PAHs by approaching the size and properties of graphite is not hampered by the numerous side chains which are necessary for solubilization and processability. Concerning these topics, in the following we employ theoretical considerations and use molecular dynamics simulations (MD) which allow studying the molecular arrangement in more detail. Note, however, that MD is not capable of predicting the self-assembled structure, due to limited time and length scales it can assess, but merely scrutinizes the coherence of the model built from the experimental data.

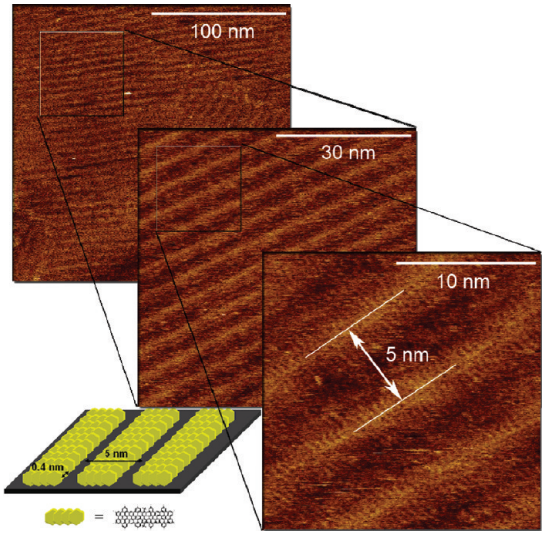

Figure 3. STM image of PAH ribbon 16 on HOPG and corresponding model of molecular arrangement of the aromatic core. The values of intracolumnar (0.4 nm) and intercolumnar (5 nm) spacing are obtained from STM measurements.

According to our previous work,[40,41] the equilibrium *torsion* angle, associated with the first bond of the alkyl side chain, counting from its attachment to the aromatic core, equals 90°. Side chains can, therefore, have two arrangements with respect to the core, with the torsion angle of 90° or −90°. Here we consider two typical side-chain orientation patterns leading to a face-to-face packing of the aromatic cores: (i) all chains on one side of the core plane in a cuplike fashion (see Figure 4a) or (ii) S-shaped, with a half of the side chains on one side and the other half on the other side of the core plane, as shown in Figure 4b. Note that the second arrangement of the side chains leads to a shift of aromatic cores with respect to each other and has already been proposed for the herringbone packing of HBCs.[41]

In the experiment, molecular aggregates are adsorbed on a HOPG surface. Since MD simulations can only reproduce the distances between the aggregates and molecules within them, but not the self-assembly itself, we can, to a reasonable approximation, consider either a fully periodic system (in this case the neighboring sheet mimics the surface) or a two-dimensional system, which would then correspond to a free-standing film of the material. We considered both cases and found that the lattice constants of prearranged self-assembled structures are not sensitive to the type of imposed periodic boundary conditions, indicating that the interaction with the surface, while crucial for self-assembly, does not change the internal structure of the layer. Below we discuss the three-dimensional case only.

To test which side chain arrangement gives the closest approximation to the experimentally measured lattice constants, we have constructed several unit cells. For the S-shaped conformation the initial unit cell dimensions were $40 \times 60 \times 8$ Å with $\alpha = 0°$, 20°, 30°, and 40°. The unit cell of a cuplike molecule had the same dimensions; the angle α was fixed at 90°. The simulation box was constructed by multiplying the unit cell by a factor of 5 in the direction perpendicular to the aromatic core and by a factor of 2 in the direction parallel to it. Two representative MD snapshots are shown in Figure 4 (simulation details are given in the Supporting Information). One can see that the molecules are

Table 2. Intercolumnar (L) and Intracolumnar (d) Distances for Different Initial Unit Cells

	d, nm	L, nm
cuplike arrangement	0.56	4.2
S-shaped, 20°	0.52	4.5
S-shaped, 30°	0.56	4.0
S-shaped, 40°	0.56	3.6

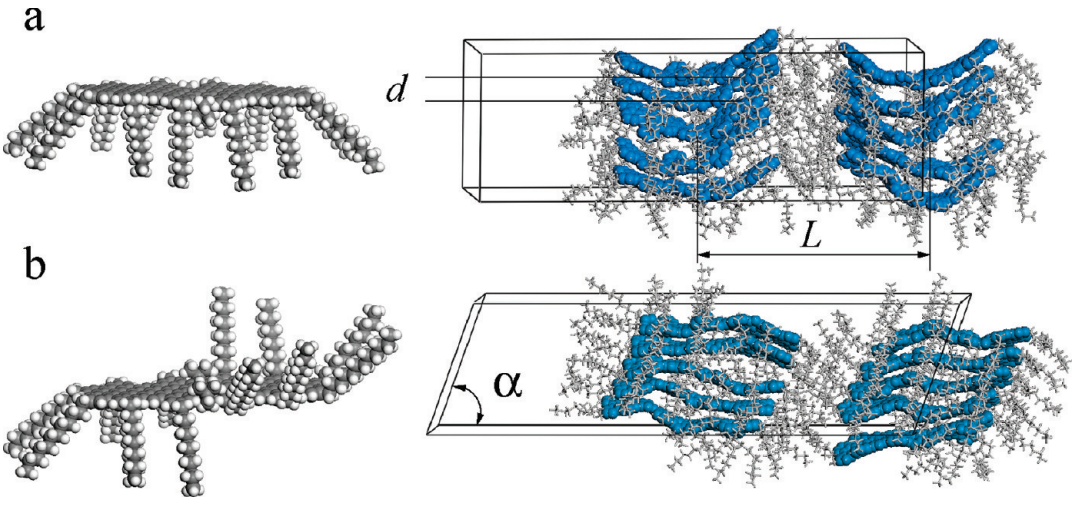

Figure 4. Possible arrangements of alkyl side chains: (a) cuplike, with all chains on one side of the aromatic core; (b) S-shaped, with a half of the side chains on one and half on the other side of the core. On the right: equilibrated columns of PAH ribbon **16**: (a) in a cuplike (b) in an S-shaped molecular conformation.

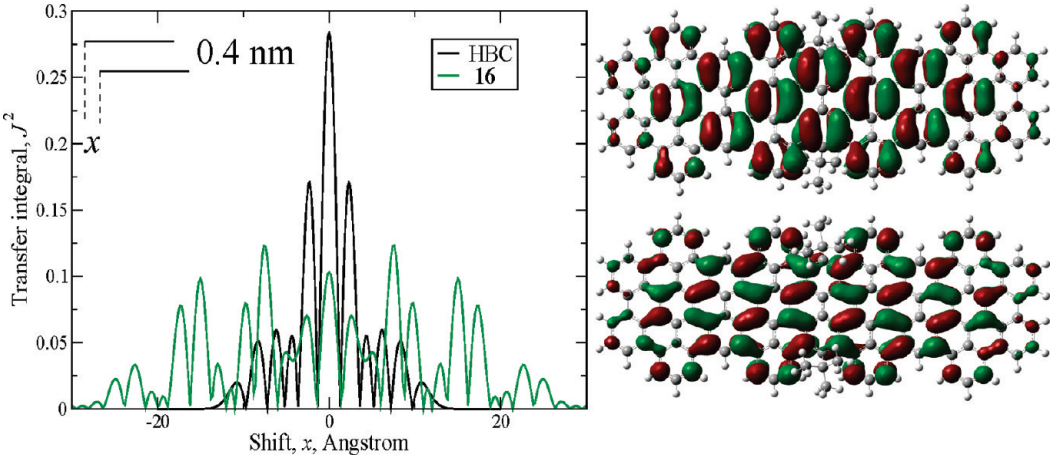

Figure 5. Left: transfer integral J for the hole transport of PAH ribbon **16** (HOMO−HOMO orbital overlap) as a function of molecular shift. The distance between the molecules was fixed at 4 Å. For comparison, we show the same integral for an HBC molecule. Right: HOMO (top) and LUMO (bottom) orbitals of 16 are clearly delocalized in spite of the distortions due to two *tert*-butyl groups.

well aligned within the columns, though the cores undergo significant distortions. By analyzing the size of the simulation box, we were able to accurately determine inter- and intracolumnar distances, which are summarized in Table 2.

The results show that the S-shaped molecular conformation with the 20° tilt angle in a column provides the closest approximation to the experimental values as well as the smallest intramolecular packing observed in simulations. This can be rationalized in terms of optimal molecular packing: a small molecular tilt angle allows shifting of the aromatic cores with respect to each other, providing a better packing of the side chains. It also helps to avoid steric overlap of bulky *tert*-butyl groups and alkyl side chains, which are present in a face-to-face geometry, similar to what is observed in a herringbone phase of HBC.

Finally, we discuss the advantages of an extended two-dimensional π-system of the cyclized compound **16** for charge transport in self-assembled structures. As a reference system, we take the PAH hexabenzocoronene (HBC). By furnishing HBC with alkyl side chains, it is possible to obtain self-assembled columnar structures. Because of the overlap of the π- orbitals of the neighboring molecules, the columns can conduct charge carriers, acting as molecular wires. Similar function can be thought of for PAH ribbon **16** self-assembled on a surface with electrodes.

The relation of the molecular structure and charge mobility in such systems has been studied recently.[42−44] The charge transport along the columns can be described within the framework of high-temperature nonadiabatic Marcus theory, which provides the rate of the charge transfer from one molecule to another[45,46]

$$\omega = \frac{J^2}{\hbar}\sqrt{\frac{\pi}{\lambda kT}}\exp\left[-\frac{\lambda}{4kT}\right]$$

where $\hbar$ is Planck's constant, k Boltzmann's constant, and T the temperature. The two main parameters governing the efficiency of transport are transfer integral J and reorganization energy λ, which can be obtained using quantum-chemical calculations (see Supporting Information for details).

For the reorganization energy of **16**, the obtained value of λ = 0.04 eV is much smaller than 0.1 eV for HBC[2] and hence favors faster hopping rates. Note that in the expression for the Marcus rate λ is in the exponent; i.e., taking into account that eV ~ 40 kT, this would lead to more than 1 order of magnitude increase of the hopping rate.

Regarding the transfer integrals, the main problem of self-assembled HBCs is the one-dimensional character of charge transport. Even when assembled on a surface, lateral shifts of the neighboring molecules in columns result in large variations (i.e., wide distribution) of transfer integrals, since the latter is an overlap of the electronic orbitals participating in charge transport. Because the molecular arrangement is intrinsically one-dimensional, the mobility is determined by the tail of *small* integrals. This implies that a shift of the order of the size of the aromatic core kills the charge transport along the whole column. The situation is of course much better for extended two-dimensional PAHs, where rather large lateral displacements still allow for a significant molecular overlap. This is illustrated in Figure 5, where the value of J as a function of the lateral molecular displacement is shown for a dimer of **16**, together with a similar dependence for an HBC dimer.[44] As expected, the interval of relative displacements at which the transfer integral is nonzero is much more extended for **16** than for HBC due to a larger conjugated core. Note that in a face-to-face geometry (zero shift) **16** has a smaller transfer integral than HBC, which is common for conjugated compounds: the increase of the size of the conjugated core at a fixed molecular separation leads, in most cases, to the decrease of the overlap integral. This decrease is nevertheless compensated by the simultaneous decrease of the reorganization energy, leading to higher hopping rates.[47,48] Summarizing, one can conclude that small reorganization energy and large overlap area of **16** should assist charge transport along the columns by increasing the absolute value of charge hopping rates and make the system less sensitive to intramolecular shifts and defects.

Conclusions

A novel chemical approach has been developed which allows for the synthesis of a homologous series of five monodispersed polyphenylene ribbons with sizes ranging from 132 (**7**) to 372 (**15**) carbon atoms in the aromatic backbone. The polyphenylene ribbons include rigid dibenzo[*e*,*l*]pyrene repeat units and were synthesized by a stoichiometrically controlled Diels−Alder reaction yielding two important compounds in a single step: one of them is a homologue of the desired series, and the other one is the starting compound for the next higher homologue. The polyphenylene ribbons are designed to serve as precursor molecules for giant PAH ribbons, which is demonstrated for the lowest homologue containing 132 carbon atoms in the aromatic core. The conversion of the polyphenylene ribbon into the PAH ribbon is achieved in a single step by cyclodehydrogenation and represents an alternative bottom-up approach toward two-dimensional nanographenes. The smallest PAH ribbon prepared by this method could be fully characterized due to its sufficient solubility in organic solvents. The molecular "sheet" as well as its

atomic lattice could be detected by HRTEM and SAED. Its self-assembly behavior induced by the aromatic interaction of the molecules was also observed by STM, which was further supported by molecular dynamics simulations. The theoretical consideration allowed to study the possible molecular arrangements and the influence of alkyl side chains in detail and provided insight into expected improvements of the intracolumnar charge transport. It turns out that the numerous alkyl substituents of **16**, decorating the aromatic core, still allow a close face-to-face packing of the conjugated systems by adopting a small molecular shift with respect to each other, thus avoiding an overlap of the bulky side chains. The calculated superior parameters of **16** (bigger nonzero transfer integral interval, lower reorganization energy) of the molecular ribbon for charge transport along the columns compared to a similar face-to-face columnar alignment of HBC molecules render it an interesting candidate for future applications in electronic devices. In general, the present work provides not only a new series of polyphenylene ribbons but also a novel strategy for the bottom-up preparation of monodispersed graphenes.

Acknowledgment. This work was financially supported by the EU Integrated Project NAIMO (No. NMP4-CT-2004-500355) and the Max-Planck-Society through the program ENERCHEM. Financial support from Deutsche Forschungsgemeinschaft (DFG) priority program SSP 1355 "Elementary Processes of Organic Photovoltaics" is gratefully acknowledged. We thank Prof. Zhaohui Wang, Dr. Marcel Kastler, and Dr. Frédéric Laquai for helpful discussions. D. Andrienko acknowledges DFG for the financial support. We thank Mr. Qi Su for his synthetic support.

Supporting Information Available: Experimental section, spectroscopic properties of polyphenylene ribbons, TEM of **15**, and molecular dynamics simulations. This material is available free of charge via the Internet at http://pubs.acs.org.

References and Notes

(1) Kastler, M.; Pisula, W.; Wasserfallen, D.; Pakula, T.; Mullen, K. *J. Am. Chem. Soc.* **2005**, *127* (12), 4286–4296.
(2) Lemaur, V.; Da Silva Filho, D. A.; Coropceanu, V.; Lehmann, M.; Geerts, Y.; Piris, J.; Debije, M. G.; Van de Craats, A. M.; Senthilkumar, K.; Siebbeles, L. D. A.; Warman, J. M.; Bredas, J. L.; Cornil, J. *J. Am. Chem. Soc.* **2004**, *126* (10), 3271–3279.
(3) Meijer, E. W.; Schenning, A. *Nature* **2002**, *419* (6905), 353–354.
(4) Boncheva, M.; Whitesides, G. M. *Adv. Mater.* **2005**, *17* (5), 553.
(5) Schmidt-Mende, L.; Fechtenkötter, A.; Müllen, K.; Moons, E.; Friend, R. H.; MacKenzie, J. D. *Science* **2001**, *293* (5532), 1119–1122.
(6) Hoeben, F. J. M.; Jonkheijm, P.; Meijer, E. W.; Schenning, A. *Chem. Rev.* **2005**, *105* (4), 1491–1546.
(7) Love, J. C.; Estroff, L. A.; Kriebel, J. K.; Nuzzo, R. G.; Whitesides, G. M. *Chem. Rev.* **2005**, *105* (4), 1103–1169.
(8) Sakamoto, Y.; Suzuki, T.; Miura, A.; Fujikawa, H.; Tokito, S.; Taga, Y. *J. Am. Chem. Soc.* **2000**, *122* (8), 1832–1833.
(9) Alameddine, B.; Aebischer, O. F.; Amrein, W.; Donnio, B.; Deschenaux, R.; Guillon, D.; Savary, C.; Scanu, D.; Scheidegger, O.; Jenny, T. A. *Chem. Mater.* **2005**, *17* (19), 4798–4807.
(10) Bock, H.; Rajaoarivelo, M.; Clavaguera, S.; Grelet, E. *Eur. J. Org. Chem.* **2006**, *13*, 2889–2893.
(11) Arnold, F. E.; Vandeuse, Rl *Macromolecules* **1969**, *2* (5), 497.
(12) Arnold, F. E.; Vandeuse, Rl *J. Appl. Polym. Sci.* **1971**, *15* (8), 2035.
(13) Sicree, A. J.; Vandeuse, Rl; Arnold, F. E. *J. Polym. Sci., Part A: Polym. Chem.* **1974**, *12* (2), 265–272.
(14) Vandeuse, Rl *J. Polym. Sci., Part B: Polym. Lett.* **1966**, *4* (3), 211.
(15) Imai, K.; Kurihara, M.; Mathias, L.; Wittmann, J.; Alston, W. B.; Stille, J. K. *Macromolecules* **1973**, *6* (2), 158–162.
(16) Stille, J. K.; Freeburg, .Me. *J. Polym. Sci., Part B: Polym. Lett.* **1967**, *5* (11), 989.
(17) Stille, J. K.; Mainen, E. L. *J. Polym. Sci., Part B: Polym. Lett.* **1966**, *4* (9), 665.
(18) Deschryv, F.; Marvel, C. S. *J. Polym. Sci., Part A: Polym. Chem.* **1967**, *5* (3), 545.
(19) Kellman, R.; Marvel, C. S. *J. Polym. Sci., Part A: Polym. Chem* **1975**, *13* (9), 2125–2131.
(20) Murphy, A. R.; Frechet, J. M. J.; Chang, P.; Lee, J.; Subramanian, V. *J. Am. Chem. Soc.* **2004**, *126* (6), 1596–1597.
(21) Wu, J. S.; Grimsdale, A. C.; Mullen, K. *J. Mater. Chem.* **2005**, *15* (1), 41–52.
(22) Wu, J. S.; Gherghel, L.; Watson, M. D.; Li, J. X.; Wang, Z. H.; Simpson, C. D.; Kolb, U.; Müllen, K. *Macromolecules* **2003**, *36* (19), 7082–7089.
(23) Watson, M. D.; Fechtenkötter, A.; Müllen, K. *Chem. Rev.* **2001**, *101* (5), 1267–1300.
(24) Fechtenkötter, A.; Saalwaechter, K.; Harbison, M. A.; Müllen, K.; Spiess, H. W. *Angew. Chem., Int. Ed.* **1999**, *38*, 3039–3042.
(25) Dotz, F.; Brand, J. D.; Ito, S.; Gherghel, L.; Mullen, K. *J. Am. Chem. Soc.* **2000**, *122* (32), 7707–7717.
(26) Iyer, V. S.; Wehmeier, M.; Brand, J. D.; Keegstra, M. A.; Mullen, K. *Angew. Chem., Int. Ed.* **1997**, *36* (15), 1604–1607.
(27) Iyer, V. S.; Yoshimura, K.; Enkelmann, V.; Epsch, R.; Rabe, J. P.; Mullen, K. *Angew. Chem., Int. Ed.* **1998**, *37* (19), 2696–2699.
(28) Samori, P.; Fechtenkotter, A.; Jackel, F.; Bohme, T.; Mullen, K.; Rabe, J. P. *J. Am. Chem. Soc.* **2001**, *123* (46), 11462–11467.
(29) Stabel, A.; Herwig, P.; Mullen, K.; Rabe, J. P. *Angew. Chem., Int. Ed.* **1995**, *34* (15), 1609–1611.
(30) Berresheim, A. J.; Müller, M.; Müllen, K. *Chem. Rev.* **1999**, *99* (7), 1747–1785.
(31) Fogel, Y.; Kastler, M.; Wang, Z. H.; Andrienko, D.; Bodwell, G. J.; Mullen, K. *J. Am. Chem. Soc.* **2007**, *129* (38), 11743–11749.
(32) Wasserfallen, D.; Kastler, M.; Pisula, W.; Hofer, W. A.; Fogel, Y.; Wang, Z. H.; Müllen, K. *J. Am. Chem. Soc.* **2006**, *128* (4), 1334–1339.
(33) Feng, X. L.; Wu, J. S.; Ai, M.; Pisula, W.; Zhi, L. J.; Rabe, J. P.; Mullen, K. *Angew. Chem., Int. Ed.* **2007**, *46* (17), 3033–3036.
(34) Clar, E. *Polycyclic Hydrocarbons*; New York, 1964; Vol. *1*, p 2.
(35) Fetzer, J. C. *Large* ($C \geq 24$) *Polycyclic Aromatic Hydrocarbons*; John Wiley & Sons: New York, 2000.
(36) Gaussian 03: Frisch, M. J.; Trucks, G. W.; Schlegel, H. B.; Scuseria, G. E.; Robb, M. A.; Cheeseman, J. R.; Montgomery, J. A., Jr.; Vreven, T.; Kudin, K. N.; Burant, J. C.; Millam, J. M.; Iyengar, S. S.; Tomasi, J.; Barone, V.; Mennucci, B.; Cossi, M.; Scalmani, G.; Rega, N.; Petersson, G. A.; Nakatsuji, H.; Hada, M.; Ehara, M.; Toyota, K.; Fukuda, R.; Hasegawa, J.; Ishida, M.; Nakajima, T.; Honda, Y.; Kitao, O.; Nakai, H.; Klene, M.; Li, X.; Knox, J. E.; Hratchian, H. P.; Cross, J. B.; Adamo, C.; Jaramillo, J.; Gomperts, R.; Stratmann, R. E.; Yazyev, O.; Austin, A. J.; Cammi, R.; Pomelli, C.; Ochterski, J. W.; Ayala, P. Y.; Morokuma, K.; Voth, G. A.; Salvador, P.; Dannenberg, J. J.; Zakrzewski, V. G.; Dapprich, S.; Daniels, A. D.; Strain, M. C.; Farkas, O.; Malick, D. K.; Rabuck, A. D.; Raghavachari, K.; Foresman, J. B.; Ortiz, J. V.; Cui, Q.; Baboul, A. G.; Clifford, S.; Cioslowski, J. ; Stefanov, B. B.; Liu, G.; Liashenko, A.; Piskorz, P.; Komaromi, I.; Martin, R. L.; Fox, D. J.; Keith, T.; Al-Laham, M. A.; Peng, C. Y.; Nanayakkara, A.; Challacombe, M.; Gill, P. M. W.; Johnson, B.; Chen, W.; Wong, M. W.; Gonzalez, C.; Pople, J. A. Gaussian, Inc., Pittsburgh, PA, **2003**.
(37) Parac, M.; Grimme, S. *Chem. Phys.* **2003**, *292* (1), 11–21.
(38) Horiuchi, S.; Gotou, T.; Fujiwara, M.; Asaka, T.; Yokosawa, T.; Matsui, Y. *Appl. Phys. Lett.* **2004**, *84* (13), 2403–2405.
(39) Meyer, J. C.; Geim, A. K.; Katsnelson, M. I.; Novoselov, K. S.; Booth, T. J.; Roth, S. *Nature* **2007**, *446* (7131), 60–63.
(40) Marcon, V.; Vehoff, T.; Kirkpatrick, J.; Jeong, C.; Yoon, D. Y.; Kremer, K.; Andrienko, D. *J. Chem. Phys.* **2008**, *129*, 094505.
(41) Carminati, M.; Brambilla, L.; Zerbi, G.; Muellen, K.; Wu, J. S. *J. Chem. Phys.* **2005**, *123*, 14.
(42) Feng, X.; Marcon, V.; Pisula, W.; Hansen, M. R.; Kirkpatrick, J.; Grozema, F.; Andrienko, D.; Kremer, K.; Mullen, K. *Nat. Mat.* **2009**, *421*, 8.
(43) Kirkpatrick, J.; Marcon, V.; Kremer, K.; Nelson, J.; Andrienko, D. *J. Chem. Phys.* **2008**, *129*, 9.
(44) Kirkpatrick, J.; Marcon, V.; Nelson, J.; Kremer, K.; Andrienko, D. *Phys. Rev. Lett.* **2007**, *98* (22), 227402.
(45) Freed, K. F.; Jortner, J. *J. Chem. Phys.* **1970**, *52* (12), 6272.
(46) Marcus, R. A. *Rev. Mod. Phys.* **1993**, *65* (3), 599–610.
(47) Bredas, J. L.; Calbert, J. P.; da Silva, D. A.; Cornil, J. *Proc. Natl. Acad. Sci. U.S.A.* **2002**, *99* (9), 5804–5809.
(48) Bredas, J. L.; Beljonne, D.; Cornil, J.; Coropceanu, V.; da Silva, D.; Malagoli, M.; Pourtois, G.; Zojer, E. *Abstr. Pap. Am. Chem. Soc.* **2002**, *224*, U56–U56.